5. CONFORMAL MICROSTRIP SLOT ANTENNA WITH AN AMC REFLECTOR IN CLOSE PROXIMITY WITH BIO-MEDIUM/BIO-MEDIA

5.1 Introduction

A hyperthermia applicator should provide good impedance matching, minimum leakage radiation outside the targeted area, and be light in weight, flexible and compact in size. Moreover, hyperthermia applicator should remain sufficiently matched to the source during variably loaded conditions to simplify the overall system stability which is a challenging design issue. Typically, the performance of the applicator in close proximity to the tissue is very much influenced by the surrounding environment. For clinical applications, flexible applicators are usually bent around the patient's body with certain curvature. Changes in the curvature of the applicator might result in changes in heating pattern within the tissue, when the applicator is bent [Correia *et al.* (2009)]. Additionally, the depth of penetration at microwave frequencies is generally shallow, and therefore, it is difficult to heat tissues at greater depth. A lot of effort has gone into increasing the penetration depth (PD) of microwave in the tissue using different types of waveguide applicators. However, waveguide applicators are heavy, large in size and have fixed form of aperture. Use of microstrip antenna applicator may solve most of these problems, because it is small in size, flexible and light in weight [Montecchia (1992)]. Various microstrip antennas including the ring radiator [Bahl *et al.* (1980)b], loop radiator [Bahl *et al.* (1982)], compact patch [Curto *et al.* (2009)] and slot antennas [Bahl *et al.* (1980)a, Koo *et al.* (2014)] were investigated for hyperthermia. Only few papers on microstrip slot antenna designed at 2.45 GHz have been published by researchers [Bahl *et al.* (1980)a, Bahl *et al.* (1980)b] to effectively heat small tumors. Several approaches can be used to improve the efficacy of the conventional microstrip patch antenna for hyperthermia. The use of a slot antenna and microstrip feedline improves the bandwidth, effective field size (EFS) and PD [Koo *et al.* (2014)]. However, slot antenna has bidirectional radiation which leads to safety concerns. Several

techniques have been reported to solve the said problem including the use of back shield and conducting ground plane. In reference [Koo *et al.* (2014)], back shield made of neoprene has been used to limit the back radiation. The applicator consists of many layers, with embedded feeding, which makes the antenna geometry complex, and therefore, it is not easy to handle. In reference [Bahl *et al.* (1980)a], conducting ground plane at fixed distance equal to a quarter-wavelength from the antenna structure has been used to eliminate back side radiation, which makes the applicator of large profile. If the reflector distance is reduced to achieve a lower profile, impedance matching deteriorates. To surmount this problem, an artificial magnetic conductor (AMC) reflector (which emulates a perfect magnetic conductor (PMC) in particular frequency band) can be used whose in-phase reflection characteristic enhances the gain of the antenna and suppresses the back field [Elek *et al.* (2005)]. Therefore, an AMC may be the better option to suppress back field/redirect the back field constructively toward the patient in hyperthermia treatment for low profile applicators. In this respect, a low profile antenna-AMC combination having wide bandwidth, enhanced PD and reduced backfield radiation is highly appreciated. To the best of author's knowledge, little work has been done on the slot antenna-AMC combination to treat small tumors at 2.45 GHz. The characteristics of conventional slot antenna with AMC in free space are described in the literature [Elek *et al.* (2005), Joubert *et al.* (2012), Agarwal *et al.* (2013), EL-Genedy *et al.* (2014)] but its application to hyperthermia has not been explored yet.

In this chapter, the simulation and experimental studies of a new microstrip slot antenna integrated with a novel and compact AMC reflector designed at 2.45 GHz for hyperthermia application is presented. The input characteristics along with near field distribution of the proposed antenna with AMC in presence of phantom bio-medium and SAR distributions in phantom muscle medium due to the applicator are investigated. The proposed antenna integrated with the AMC is designed to effectively radiate into the muscle medium. The AMC structure is utilized to provide in-phase reflection, which significantly enhances the front-to-back ratio and consequently enhances the PD in the muscle medium. Further, the

input characteristics and SAR parameters for the proposed antenna without AMC, conventional rectangular patch antenna without AMC, and the proposed antenna-AMC and the antenna-conventional perfect electric conductor (PEC) combinations in proximity with phantom bio-medium are also compared. Furthermore, the effect of variation in the dielectric property of bio-medium on the input reflection coefficient-frequency characteristic of the proposed antenna with AMC is also studied through simulation. The reflection coefficient-frequency characteristic of the applicator and normalized SAR distributions in phantom muscle medium due to the applicator with AMC were also determined experimentally and the experimental results are compared with the respective simulation results. Thermal simulation was also performed for the realistic tri-layered and five-layered bio-models without and with oval-/irregular-shaped tumor, which is in close proximity with the antenna-AMC combination. In addition, the effects of change in the radius of curvature of proposed applicator and bio-model on E-field distribution and SAR distributions/temperature distributions in homogeneous/tri-layered/five-layered bio-models are investigated through simulation. Simulation study was carried out using computer simulation technology microwave studio (CST MWS) 2011 software, which is based on finite integration numerical technique.

5.2 Antenna configuration

The configuration of the proposed antenna along with its fabricated prototype and detailed dimensions is shown in Figure 5.1. The basic idea about the design of proposed applicator is taken from reference [Koo *et al.* (2014)] in which a complex multilayered geometry with embedded feeding is used.

The proposed microstrip slot antenna has simple geometry and consists of two circular conducting parasitic patches enclosed within a modified rectangular slot. The rectangular slot of the proposed antenna is modified by rounding the corners of the slot, which is etched on the ground plane of size 29 mm × 29 mm to enhance the impedance bandwidth of the proposed antenna. The slot is fed by a 50 Ω tapered microstrip line with curved tuning stub, which is printed on opposite

side of the RT duroid substrate having ε_r' of 2.2, tanδ of 0.0009 and thickness of 0.508 mm and placed symmetrically with respect to y-axis as shown in Figure 5.1. The parameters of the modified ground plane and feed are optimized for maximum PD in muscle medium/multi-layered bio-media and minimum input reflection coefficient at the operating frequency of 2.45 GHz. The optimized dimensions of the proposed antenna are given in Figure 5.1(a).

The proposed antenna of optimum geometrical dimensions was fabricated with the help of LPKF ProtoMat S103 PCB prototyping machine for the validation of the optimized simulation results. Top and bottom views of the fabricated prototype of the proposed antenna are shown in Figure 5.1(b).

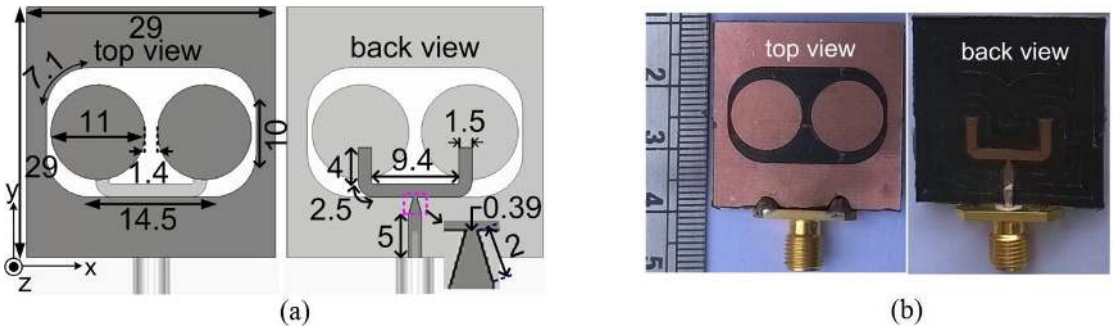

Figure 5.1: Proposed antenna geometry (a) top and back views, and (b) fabricated prototype. (All dimensions are in mm)

5.3 Iteration steps involved in the design of proposed antenna and performance comparison with the conventional rectangular patch antenna

Simulations were performed for different configurations of the slot antenna and conventional rectangular patch antenna fed through 50 Ω microstrip line for comparison of their performances. Identical substrate material–RT duroid 5880 (ε_r' = 2.2, tanδ = 0.0009 and thickness = 0.508 mm) and antenna-muscle separation (= 5 mm) were taken in the simulation study for all the configurations of the antenna (Figure 5.2).

5.3.1 *Reflection coefficient-frequency characteristics*

Parametric studies were performed to analyse the effects of various design parameters on input reflection coefficient-frequency characteristics of the antenna/s including the proposed antenna. For the simulation study of input

reflection coefficient-frequency characteristics, four antenna configurations (Antenna1, Antenna2, Antenna3, and Antenna4) shown in Figure 5.3 were considered. Antenna1 consists of two circular parasitic patches, each of diameter 11 mm enclosed within a rectangular slot of size 25 mm ×15 mm etched on ground plane of size 29 mm × 29 mm. The slot antenna is fed by a 50 **Ω** microstrip line printed on the opposite side of the substrate and placed centrally as shown in Figure 5.3. The configuration of Antenna2 is similar to that of Antenna1 excepting the corners of rectangular slot, which are rounded in Antenna2. The dimensional details of rounded corners in the configuration of Antenna2 are shown in Figure 5.3. The configuration of Antenna3 is that of Antenna1 with modified feed. The straight microstrip line feed of Antenna1 was converted into modified tapered feed with curved tunning stub in Antenna3. The dimensional details of modified feed of Antenna3 are given in Figure 5.3. Withal, the modifications incorporated in Antenna2 and Antenna3 with respect to Antenna1 are integrated in Antenna4. Therefore, configuration of Antenna4, which is the proposed antenna includes modified rectangular slot of Antenna2 and modified feed provided in Antenna3 as shown in Figure 5.3. The simulated input reflection coefficient-frequency characteristics of four antennas (Antenna1, Antenna2, Anntenna3 and Antenna4) are shown in Figure 5.4. It can be observed from Figure 5.4 that for all antenna configurations, adequate impedance matching is obtained at 2.45 GHz, which is a good indication of design insensitivity to detuning caused by tissue loading. Additionally, it is also noted that the fourth antenna configuration (Antenna4) of microstrip slot antenna provides maximum impedance bandwidth (Table 5.1). Therefore, Antenna4 is selected for the application under consideration.

In order to compare the performance of the proposed antenna (Antenna4) with conventional rectangular patch antenna, simulation was also performed for the conventional rectangular patch antenna (designed at 2.45 GHz) whose configuration is shown in Figure 5.5. The simulated reflection coefficient-frequency characteristic of the conventional rectangular patch antenna is depicted in Figure 5.4, in which the simulated reflection coefficient-frequency

characteristics of four antennas (Antenna1, Antenna2, Antenna3 and Antenna4) studied earlier are also presented. The impedance bandwidths of the antennas extracted from Figure 5.4 along with the size of all antennas are presented in Table 5.1. From Table 5.1, it can be observed that Antenna 4 is smaller in size and provides impedance matching with the biological phantom (muscle) over wider frequency range as compared with the conventional patch antenna resonating at 2.45 GHz for antenna-muscle separation of 5 mm. This reveals the compactness of Antenna4 (the proposed antenna).

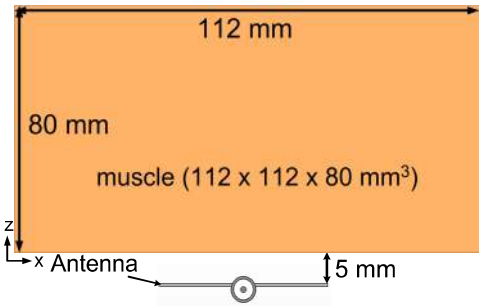

Figure 5.2: Antenna in close proximity with phantom bio-medium.

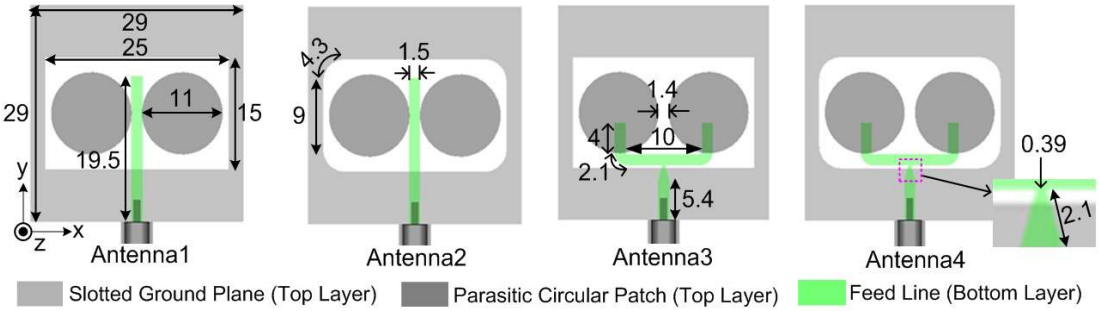

Figure 5.3: Different antenna configurations with various combinations of slotted ground plane and feed.

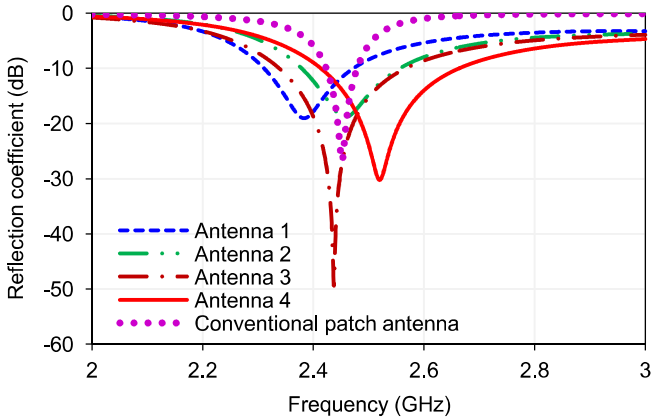

Figure 5.4: Simulated variations of input reflection coefficient of various antenna configurations and conventional rectangular patch antenna versus frequency.

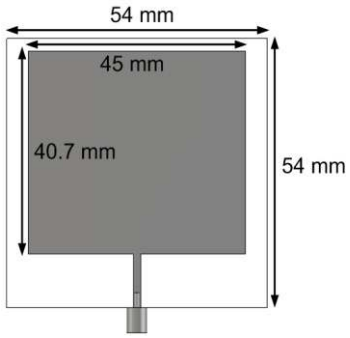

Figure 5.5: Configuration of the conventional rectangular patch antenna designed at 2.45 GHz.

5.3.2 *SAR distributions*

The simulated relative SAR distributions inside the planar phantom muscle medium of size 112 mm × 112 mm × 80 mm at 2.45 GHz due to various configurations of slot antenna and conventional rectangular patch antenna are determined using CST MWS software and the results are shown in Figure 5.6. Initially, the power fed to the antenna was assumed to be 1W in the simulation study. The relative SAR distributions in the phantom muscle medium were obtained by normalizing the SAR values with respect to the global peak SAR value that occurs in the phantom muscle medium.

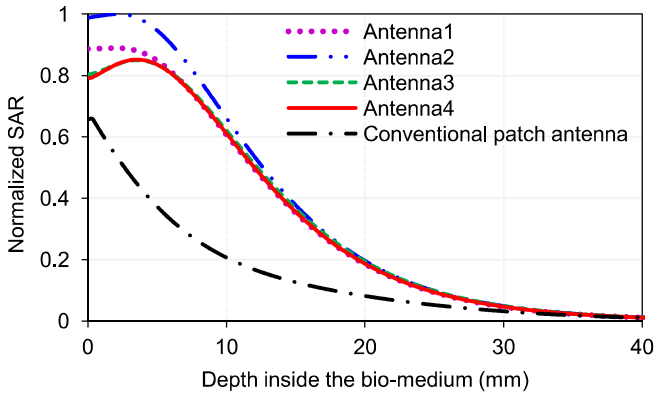

Figure 5.6: Simulated relative SAR distributions in the phantom muscle medium along z-direction (x =y = 0) due to various configurations of microstrip slot antenna and conventional microstrip patch antenna.

Figure 5.6 illustrates the relative SAR distributions in the homogeneous phantom muscle medium in z-direction for various configurations of slot antenna and conventional rectangular patch antenna. The simulated values of PD (depth where relative SAR value is down to 13.5 percent of the maximum in the muscle) inside the phantom bio-medium due to various configurations of slot antenna and

conventional rectangular patch antenna extracted from Figure 5.6 are listed in Table 5.1. It is observed from Table 5.1 that configuration designated as Antenna4 provides reasonable PD in the phantom muscle medium. Further, the results indicate that Antenna4 provides higher PD and appropriate peak SAR value as compared with conventional rectangular patch antenna.

Table 5.1: SAR parameters and -10 dB reflection coefficient bandwidth for various antenna configurations

Configuration type	Antenna size (mm^2)	Bandwidth (MHz)	PD (mm)
Antenna1	29 × 29	163	23.1
Antenna2	29 × 29	180	22.7
Antenna3	29 × 29	232	23.8
Antenna4	29 × 29	253	23.6
Conventional patch antenna	54 × 54	50	18

5.3.3 *Electric field distributions*

To compare the electric field generated in various configurations of the microstrip slot antenna, near E-field distributions in xz-plane were obtained through simulation (Figure 5.7). It is observed that back field is present in all the configurations of the slot antenna since slot antenna is a bidirectional antenna. It is essential to eliminate or redirect the back radiation of the slot antennas towards the bio-medium since it is undesirable and it would also be harmful to the operator of the hyperthermia applicator. In our implementation, an AMC reflector is used in combination with the proposed antenna configuration (Antenna4) to suppress the back field and to direct the back field towards the bio-medium.

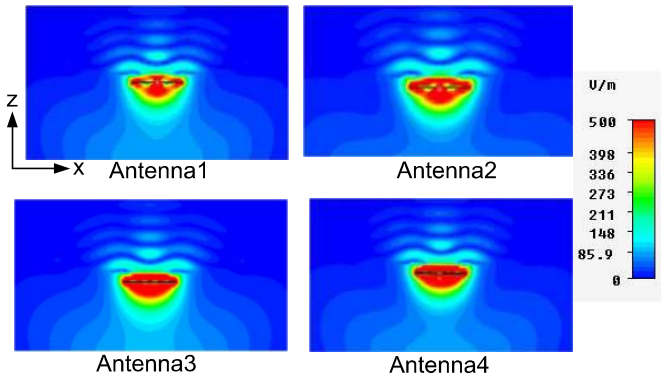

Figure 5.7: Near E-field distributions in xz-plane from various configurations of the slot antenna radiating into phantom bio-medium.

5.4 AMC configuration and its reflection phase profile

It is well known that a PEC has a reflection phase of 180^o for a normally incident plane wave, while a PMC has a 0^o reflection phase. According to image theory, a PEC ground plane causes the antenna current and its image to cancel each other, which makes the real part of the structure impedance to go to zero, while the imaginary part of impedance tends to infinity. Hence, a significant amount of energy is trapped between the antenna and the ground plane, which in turn leads to significant reduction in antenna efficiency. If an AMC reflector is used, its in-phase reflection characteristic enhances the gain of the antenna. In the application under consideration, the AMC reflector is used to suppress the backfield and to enhance the heating depth in the phantom muscle medium.

In the recent past, various AMC shapes have been discussed in terms of their reflection phase characteristics [Foroozesh *et al.* (2011)]. It is discussed in reference [Foroozesh *et al.* (2011)] that by changing the geometry of AMC, the resonant frequency of the unit cell can be changed since the value of associated reactance changes. The resonant frequency of the unit cell structure is given by

$$f_r = 1/2\pi\sqrt{LC}$$

where L and C are the effective inductance and capacitance of the structure respectively. The operating bandwidth of an AMC is defined as the difference between two frequencies on either side of the resonant frequency where its reflection phase changes from $+90^o$ to -90^o since in this range the phase values would not cause destructive interference between the direct and reflected waves. Moreover, outside this frequency band, the AMC behaves like a PEC [Feresidis *et al.* (2005)].

The description of frequency selective surfaces (FSS) based on ring type geometry is available in the literature. It is found that ring type metallization has smaller dimensions of AMC unit cells as compared with other geometries [Foroozesh *et al.* (2011)]. In the present study, a ring type AMC is modified by changing its reactance through the addition of rectangular conducting patches of different sizes to make the structure of the unit cell compact. An effective and

confirmable hyperthermia applicator with enhanced PD is designed through the combination of modified AMC and modified slot antenna.

Figure 5.8(a) and (b) shows the gradual transformation from the unit cell of square patch to the proposed AMC structure. The AMC reflector comprises 4 × 4 unit cells of modified ring AMC of size 64 mm × 64 mm printed on RT duroid substrate (ε_r = 2.2, tanδ = 0.0009) with thickness of 1.575 mm as shown in Figure 5.8(c).

The square patch acts as the basic structure for the design of the proposed AMC. Figure 5.9(a) shows the reflection phase profiles of the aforesaid structures. It can be seen from reflection phase profiles shown in Figure 5.9(a) that the square patch of size 16 mm × 16 mm results in the resonant frequency of 4.6 GHz.

The geometry of square patch is modified in the form of ring as given in reference [Foroozesh *et al.* (2011)]. Referring to reflection phase profiles given in Figure 5.9(a), it can be said that the ring geometry lowers the resonant frequency down to 3 GHz. This is due to the fact that ring geometry causes an increase in its C value, and therefore reduction in its resonant frequency [Hosseinipanah and Wu (2009)].

The ring geometry is further modified by adding rectangular conducting patches of different sizes, which results in further increase in C value, and reduction in resonant frequency down to 2.45 GHz. Therefore, it can be said that the proposed AMC design makes the structure of unit cell compact.

It is noted from reflection phase profiles depicted in Figure 5.9(a) that the resonant frequency of the proposed structure is scaled down by 53% and 82% with respect to those for square patch and ring AMCs respectively. The reflection phase profiles of the proposed AMC for transverse electric (TE) and transverse magnetic (TM) polarized incident waves are shown in Figure 5.9(b). Identical reflection phase profiles for both TE and TM polarized EM waves are observed, which proves that the reflection phase profile of the proposed AMC is insensitive to polarization of the wave.

To demonstrate the polarization insensitivity of the proposed AMC, the results of reflection phase for normal incidence for different polarization angles

'ϕ' are also shown in Figure 5.9(c). It can be observed from Figure 5.9(c) that reflection phase changes to a small extent with variation in the polarization angle. It proves that the proposed AMC is insensitive to EM wave having different polarization angles. Further, variation of reflection phase of the proposed AMC with incident angle 'θ' of EM wave was also studied. The simulated results are shown in Figure 5.9(d) for both TE and TM polarized waves. For TM wave, the reflection phase remains in the range -90° to +90° for variation in the incident angle 'θ' over the range 0–30°. But for TE wave, the reflection phase is found to vary in the range -90° to +90° when the incident angle 'θ' changes from 0 to 26°. It proves that proposed AMC can work well with incident angle ranging from 0 to 26°.

5.5 Antenna along with AMC in close proximity with phantom bio-medium

Having selected the configuration of the slot antenna (Antenna 4) as the proposed antenna, simulation study of the selected antenna configuration with a 4×4 AMC reflector as a back plane was continued. It was observed during simulation study that the presence of AMC surface reduces the resonant frequency of the applicator to some extent. Consequently, a little trimming in the dimensions of slot antenna was carried out to obtain the desired simulated reflection coefficient-frequency characteristic of the proposed antenna with AMC. The detailed dimensions of the proposed modified slot antenna are given in Figure 5.1(a). It is worth mentioning that the proposed antenna is separated from the AMC by 4 mm (optimum separation at 2.45 GHz) to reduce the problem of impedance mismatch. Styrofoam of ε_r = 1.017 is used between the antenna and AMC structure to support the AMC structure. The proposed antenna with AMC (Figure 5.10) is designed and optimized to effectively radiate into the muscle medium at 2.45 GHz by keeping the antenna-muscle separation of 5 mm along with an AMC reflector located at an optimized distance (= 4 mm) behind the slot antenna.

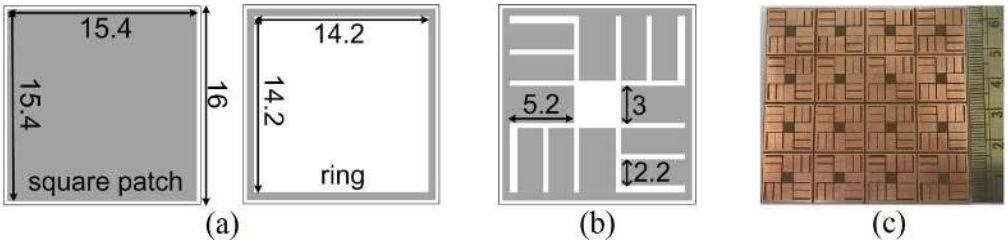

Figure 5.8: (a) Unit cell structure of square patch and ring AMCs, (b) Unit cell structure of proposed AMC, and (c) Fabricated prototype of proposed AMC reflector of 4 × 4 unit cells. (All dimensions are in mm)

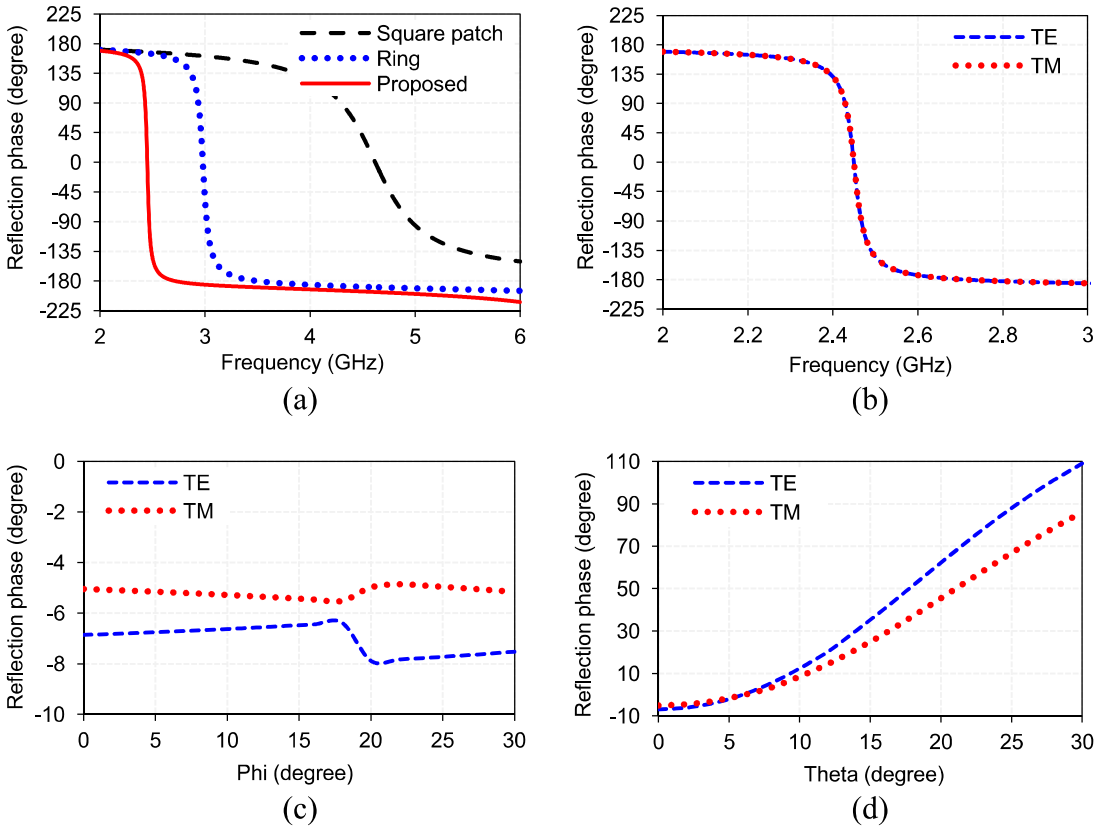

Figure 5.9: Reflection phase profiles of (a) square patch, ring and proposed AMC structure, (b) proposed AMC design for TE and TM polarizations, (c) proposed AMC for different polarization angles, and (d) proposed AMC for different angles of incidence.

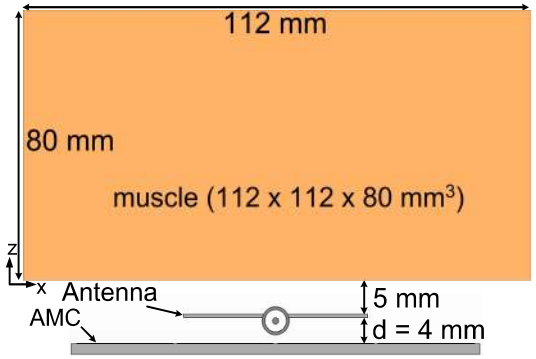

Figure 5.10: Proposed applicator with AMC terminated in phantom bio-medium.

5.5.1 *Results and discussions*

5.5.1.1 *Reflection coefficient-frequency characteristics*

In order to perceive the effect of the parameter designated as *d* (separation between the antenna and AMC) on input reflection coefficient-frequency characteristic of the proposed applicator in presence of phantom bio-medium parametric study was carried out through simulation. Figure 5.11 shows the variations of input reflection coefficient of the applicator versus frequency by taking '*d*' as a parameter. It can be observed from Figure 5.11 that as the value of *d* increases, the valley point depicting resonance condition shifts to higher frequency side. It is to be noted that optimum separation between the antenna and the AMC is 4 mm for operating frequency of 2.45 GHz.

Figure 5.12 shows the variations of both simulated and measured reflection coefficient-frequency characteristics of the proposed antenna with AMC (for optimum antenna-AMC separation of 4 mm). Measured reflection coefficient-frequency characteristic of the proposed antenna with AMC was obtained using Anritsu make vector network analyser (Model: MS203C). It is observed that measured and simulated results are nearly in agreement with each other. The slight deviation in the experimental results with respect to simulated results might have been caused due to fabrication and measurement errors.

To study the effect of change in the type of phantom bio-medium i.e. in the dielectric constant of the medium on the reflection coefficient-frequency characteristic of the proposed applicator, simulations were carried out for a wider range of real part of relative permittivity (ε_r') of the phantom bio-medium in the range 40–60, keeping the imaginary part of the relative permittivity of phantom (= 16) unaltered. The reflection coefficient-frequency characteristic of the applicator shown in Figure 5.13 indicates that the impedance matching between the proposed applicator and phantom bio-medium remains sufficiently stable when the real part of the relative permittivity ε_r' of the phantom is changed from 40 to 60. The proposed applicator's bandwidth is wide enough to tolerate such changes in dielectric property of the biological phantom.

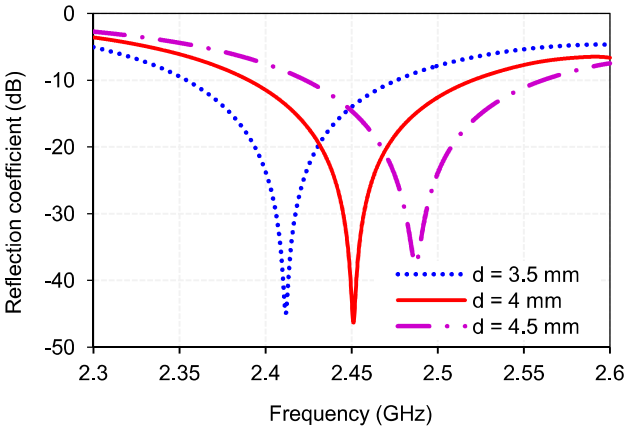

Figure 5.11: Simulated variation of input reflection coefficient of the proposed applicator versus frequency by taking antenna-AMC separation *d* as a parameter.

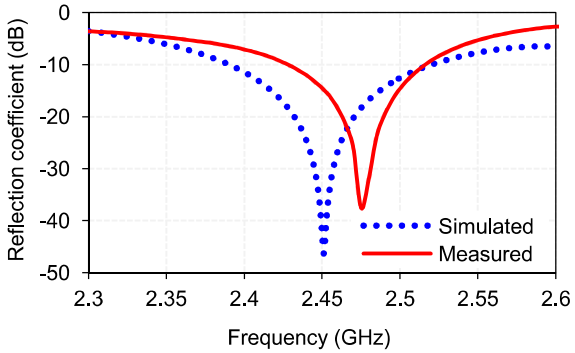

Figure 5.12: Simulated and measured variations of input reflection coefficient of the proposed antenna (with AMC) versus frequency.

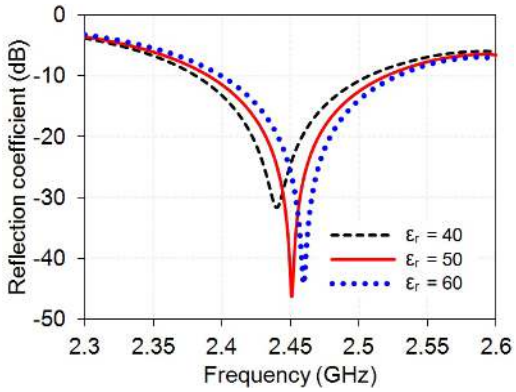

Figure 5.13: Simulated variations of input reflection coefficient of the proposed antenna with AMC versus frequency for various dielectric constant values of the phantom bio-medium.

5.5.1.2 *Electric field distributions*

To observe the electric field generated through the proposed antenna with AMC having different AMC sizes, near E-field distributions in xz-plane were obtained through simulation (Figure 5.14). It is observed that back field is present in 3×3 AMC array. However, back field is completely eliminated for 4×4 and 5×5

AMC arrays. As 5×5 AMC array increases the profile of the applicator, 4×4 AMC array (optimum array) is selected for the application under consideration. As discussed earlier, an AMC reflector at the back side of the proposed antenna prevents back radiation and directs the back electric field toward the bio-medium which is in phase with the forward electric field. This is clearly demonstrated through Figure 5.14.

5.5.1.3 *SAR distributions*

5.5.1.3.1 *Simulated SAR distributions*

The simulated relative SAR distributions inside the planar phantom muscle-medium of size 112 mm × 112 mm × 80 mm at 2.45 GHz due to the proposed antenna without and with AMC were determined using CST MWS software and the results are shown in Figure 5.15. Initially, the power fed to the antenna was assumed to be 1W in the simulation study.

5.5.1.3.2 *Experimental SAR distributions*

SAR distributions inside the phantom muscle (112 × 112 × 80 mm^3) made of 30% Gelatin + 69% Water + 1% NaCl [Stuchly and Stuchly (1980)] due to the proposed antenna with AMC were determined experimentally at 2.45 GHz as given in chapter 2. Laboratory grade gelatine and sodium chloride (NaCl) along with double distilled water were used in the preparation of the phantom (Appendix C). The experimental SAR distributions inside the phantom due to the propose applicator are shown in Figure 5.15.

5.5.1.3.3 *Comparison of simulated and experimental SAR distributions*

Figure 5.15(a) illustrates the simulated and/or experimental relative SAR distributions in the homogeneous phantom muscle medium for the proposed applicator without and with AMC. Different curves of the SAR distributions are normalized by taking respective peak absolute SAR values as reference values for normalization. That is why, value of maximum normalized SAR value for all curves is identical. The values of simulated and experimental PD in biological phantom extracted from Figure 5.15(a) are given in Table 5.2 for the proposed

antenna with and without AMC. The measured PD in the biological phantom due to the proposed antenna with AMC is nearly in agreement with the respective simulated value. Further, it is observed from Figure 5.15(a) and Table 5.2 that the presence of AMC as a back plane enhances the PD in the phantom muscle medium.

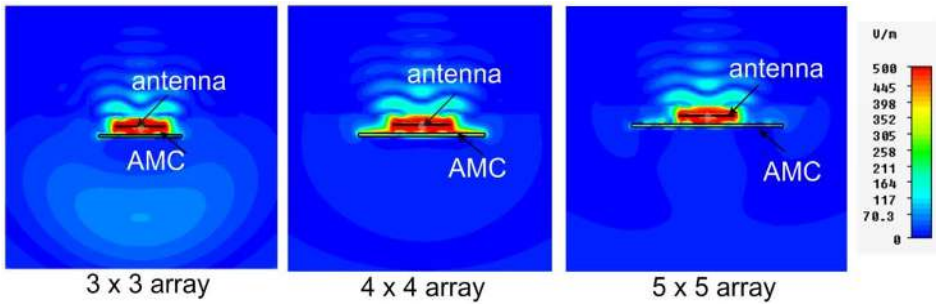

Figure 5.14: E-field distributions in xz-plane from proposed antenna with AMC for various AMC sizes, radiating into phantom bio-medium.

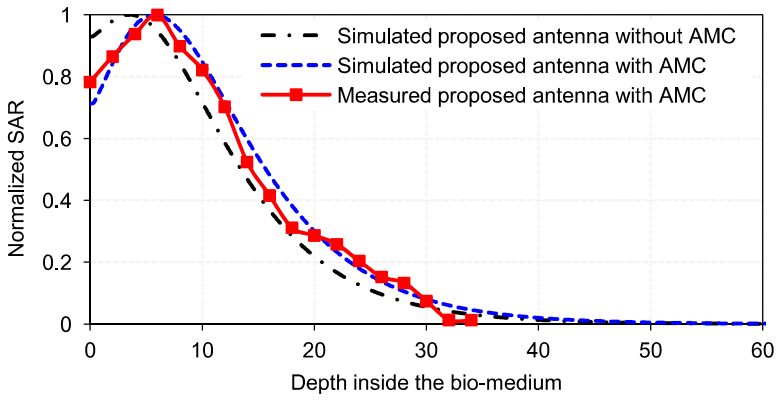

(a)

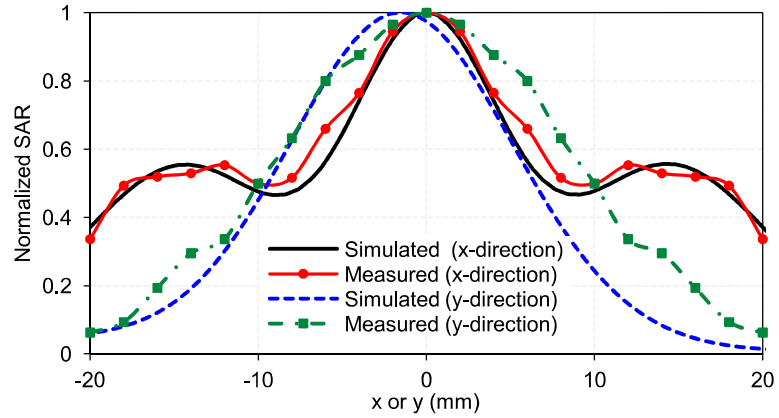

(b)

Figure 5.15: Simulated and measured variations of normalized SAR distributions in the phantom muscle medium due to proposed antenna (a) without/with AMC along z-direction (x =y = 0), and (b) with AMC along x-/y-direction (y/x = 0) at z = 10 mm.

The EFS is defined as the transverse area that is enclosed within 50% SAR contour inside the phantom bio-medium. The simulated and experimental values of EFS extracted from Figure 5.15(b) due to the proposed antenna with AMC are reasonable, and nearly in agreement with each other (Table 5.2). The EFS values obtained through simulation and measurement are reasonable for treatment of small superficial tumors.

5.5.1.4 *Comparison of antenna-AMC/PEC reflector*

In order to compare the performance of the proposed antenna-AMC and the antenna-PEC combinations, simulations were also performed for reflection coefficient-frequency characteristics of antenna-PEC combination by placing the PEC reflector at two positions behind the antenna (Figure 5.16) and the results are presented in Figure 5.17 along with the results for the antenna-AMC combination. The values of simulated -10 dB reflection coefficient bandwidth of the antenna-AMC and the antenna-PEC combinations extracted from Figure 5.17 are given in Table 5.2.

Initially the separation (*d*) between antenna and PEC was kept equal to 4 mm, same as that for the antenna-AMC combination. It can be inferred from Figure 5.17/Table5.2 that impedance matching deteriorates considerably for this antenna-PEC separation and the corresponding -10 dB reflection coefficient bandwidth becomes zero. When the PEC (conventional PEC) is placed at a separation of 30.6 mm ($0.25\lambda_o$ at 2.45 GHz) behind the antenna, good impedance matching was achieved. This is made possible due to the fact that with quarter wavelength antenna-PEC separation, the wave, which gets reflected from conventional PEC, reinforces the wave transmitted from the antenna into the bio-medium. It is to be noted here that phase reversal takes place when the wave gets reflected from a conventional PEC. This quarter wavelength antenna-PEC separation makes the applicator of large profile (Figure 5.17).

The proposed AMC kept at a distance of 4 mm ($0.03\lambda_0$ at 2.45 GHz) behind the proposed radiating element provides good impedance matching. Hence, the profile of the applicator is reduced when the proposed antenna is used in combination with the proposed AMC reflector.

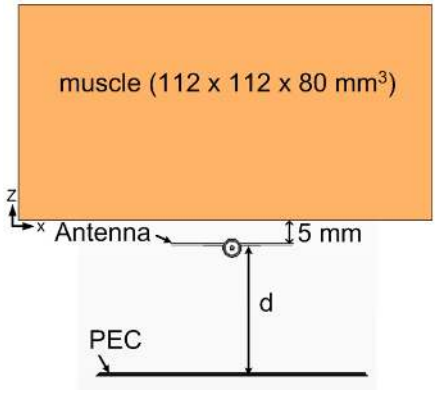

Figure 5.16: Illustration of the proposed antenna with PEC reflector.

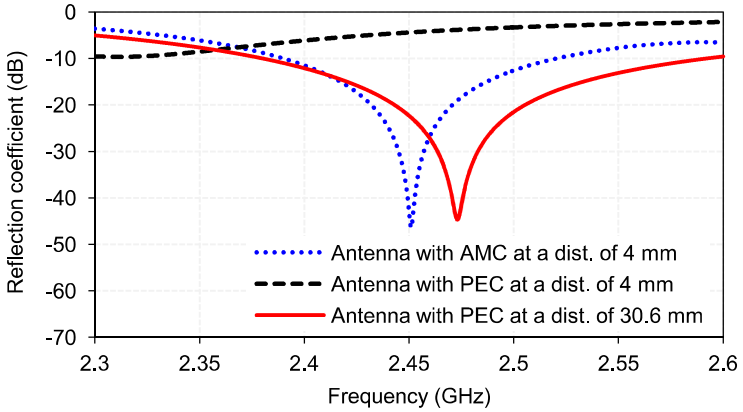

Figure 5.17: Simulated variations of input reflection coefficient of the proposed antenna with AMC/PEC versus frequency.

Moreover, it is noted from Figure 5.17/Table 5.2 that antenna-conventional PEC combination with PEC kept at a distance of 30.6 mm (0.25 λ_0 at 2.45 GHz) behind the antenna provides widest reflection coefficient bandwidth. But for the antenna-AMC combination also the bandwidth is wide enough to accommodate the detuning due to changes in dielectric property of the bio-medium.

Further, the SAR distributions due to the proposed antenna with AMC reflector and the antenna with PEC reflector were determined through simulation. Figure 5.18 illustrates the simulated relative SAR distributions in the phantom bio-medium due to different antenna-AMC/PEC combinations. The values of PD and EFS extracted from Figure 5.18 are given in Table 5.2. Moreover, it can be observed from Table 5.2 that in the presence of PEC, enhancements of PD in the bio-medium due to the proposed antenna-PEC combinations are: 1.8 mm (23.6 mm to 25.4 mm) for the antenna-PEC separation (*d*) of 4 mm, and 0.9 mm (23.6 mm to 24.5 mm) for the antenna-conventional PEC separation (*d*) of 30.6 mm.

But in the presence of AMC reflector, enhancement of PD in the bio-medium is 3.4 mm (23.6 mm to 27 mm). Hence, PD in the phantom bio-medium is enhanced due to the proposed antenna-AMC combination as compared with antenna-PEC combinations. Further, SAR values in the bio-medium for the antenna-PEC combination with PEC 4 mm behind the antenna are significantly reduced due to the existence of significant mismatch between the applicator and bio-medium. The peak values of SAR for the proposed antenna-AMC combination and the antenna-conventional PEC combination (antenna-PEC separation = $0.25\lambda_0$) are comparable. But the SAR value at the bio-surface (x = y = z = 0) due to the antenna-conventional PEC combination is close to respective peak value which may unnecessarily heat the bio-surface. In case of proposed antenna-AMC combination, SAR value at bio-surface (x = y = z = 0) is lower.

From Table 5.2 it can also be inferred that the introduction of AMC reflector not only improves the impedance matching for smaller antenna-reflector separation but also provides enhanced PD in the muscle medium. It is noted from Table 5.2 that the proposed antenna-AMC combination provides larger EFS as compared to the antenna-conventional PEC combination in which PEC is kept at 30.6 mm behind the antenna.

Table 5.2: SAR parameters and -10 dB reflection coefficient bandwidth for various antenna configurations

Configuration type		Bandwidth (MHz)	PD (mm)	EFS (mm^2)
Proposed antenna with PEC	4 mm ($0.03\ \lambda_o$)[#]	NA	25.4	37 × 15
	30.6 mm ($0.25\lambda_o$)[#]	200	24.5	14 × 17
Proposed antenna with AMC	Simulated	133	27	34 × 16
	Measured	100	28	35 × 19
Proposed antenna without AMC		253	23.6	12 × 18

[#] λ_o refers to free space wavelength at 2.45 GHz

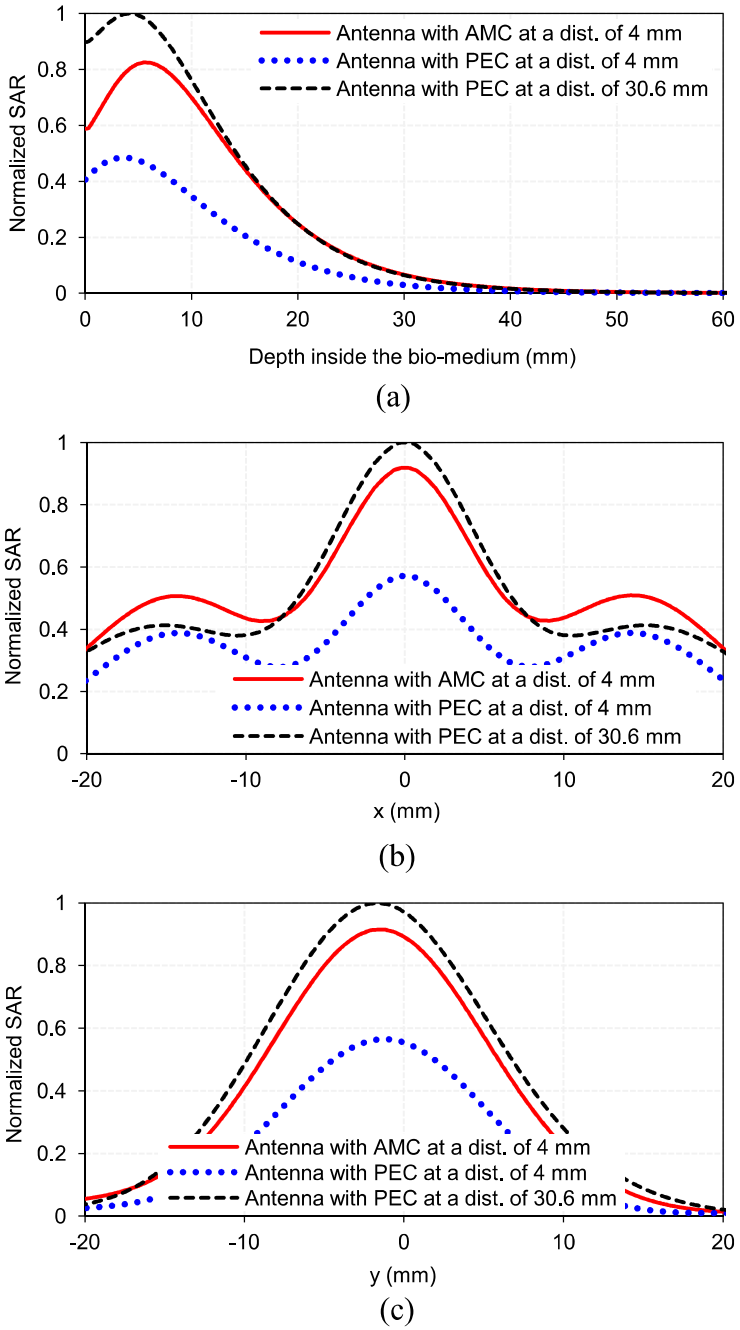

Figure 5.18: Simulated variations of normalized SAR distributions in the phantom muscle medium due to proposed antenna with AMC/PEC along (a) z-direction (x =y = 0), (b) x-direction (y = 0) at z = 10 mm, and (c) y-direction (x = 0) at z = 10 mm.

5.5.1.5 *Effects of bending*

Since the antenna is expected to be bent during the hyperthermia treatment of abdominal or curved regions of the body, simulations were conducted to study the effects of antenna curvature on near E-field distribution, applicator's input reflection coefficient-frequency characteristic and SAR distributions in homogeneous (muscle equivalent) model, which is situated close to proposed

applicator with AMC designed at 2.45 GHz. Simulations were performed for three cases: Case I pertains to both homogeneous bio-model and the proposed applicator having radius of curvature 'R' of 50 mm. Case II represents radius of curvature 'R' of 500 mm for each of the bio-model and the proposed applicator while case III involves planar bio-model and the applicator with 'R' tending to ∞.

5.5.1.5.1 *Effects of system curvature on E-field distribution*

To compare the electric field generated in the proposed antenna with AMC, near E-field distributions in xz-plane were obtained through simulation for various system's curvatures (Figure 5.19). It is observed that AMC reflector at the back side of the proposed antenna prevents back radiation and directs the back electric field toward the bio-medium for the systems' curvatures considered.

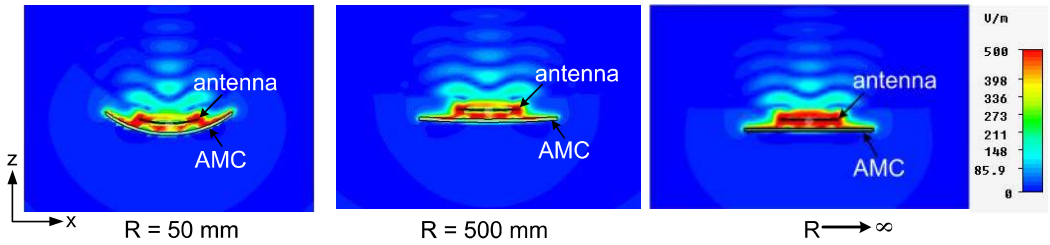

Figure 5.19: Near E-field distributions in xz-plane in the central regions of proposed antenna with AMC for different value of system's curvature, radiating into phantom bio-medium.

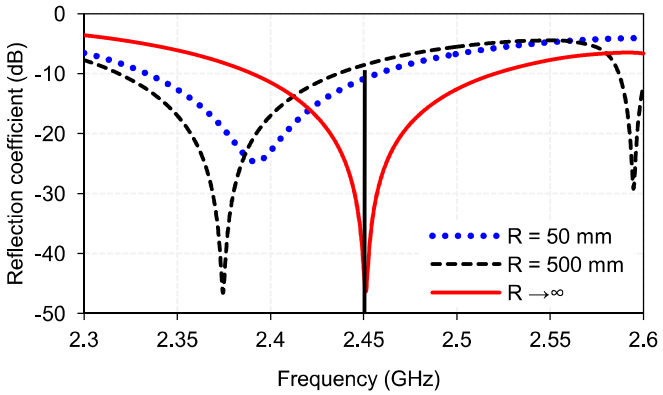

Figure 5.20: Variations of input reflection coefficient of the proposed antenna with AMC versus frequency for different values of system's radius of curvature 'R'.

5.5.1.5.2 *Effects of system's curvature on input reflection coefficient*

The variation of input reflection coefficient of the proposed antenna with AMC versus frequency was studied through simulation by taking radius of curvature 'R' of the system as a parameter. The simulation results are shown in

Figure 5.20. Figure 5.20 illustrates that reflection coefficient of the proposed applicator with AMC remains sufficiently stable at 2.45 GHz (<-9 dB) for various values of system's radius of curvature.

5.5.1.5.3 *Effect of system's radius of curvature on SAR distribution in the homogeneous bio-medium (muscle)*

Simulation study was performed for SAR distributions in the bio-medium due to the proposed applicator for various values of system's radius of curvature in the range (50 mm ≤ R ≤ ∞). Initially, power fed to the antenna was assumed to be 1 W in the simulation study. Figure 5.21 shows the SAR patterns in the xz-plane for the homogeneous muscle model of various values of radius of curvature (curvature of the applicator is identical to the bio-model). It is clear from Figure 5.21 that SAR distributions are symmetrical about z-axis and peak SAR in each case is aligned with the antenna's central axis of radiation. Tables 5.3 summarizes the SAR parameters for various values of system's radius of curvature. Further, it is observed from Figure 5.21 and Table 5.3 that SAR parameters in the bio-model don't change significantly when radius of curvature 'R' is changed from 50 mm to ∞.

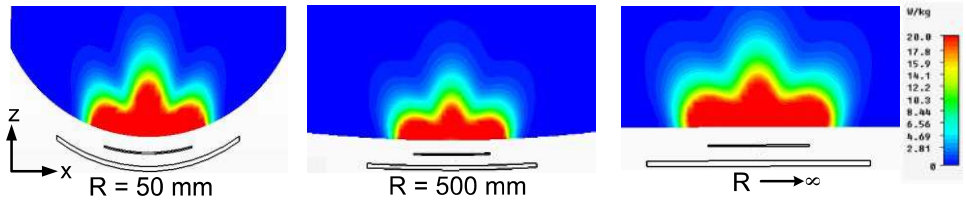

Figure 5.21: SAR patterns in muscle tissue for various values of radius of curvature of the bio-model/proposed antenna.

Table 5.3: Peak SAR and PD in the homogeneous muscle model for various values of system's radius of curvature

Curvature (mm)	Peak SAR (W/kg)	PD (mm)
R = 50	43.732	21.45
R = 500	26.6	26.4
R → ∞ (planar)	29.93	27

The results of variation in EFS in the bio-medium due to changes in the system's radius of curvature 'R' are presented in Figure 5.22. It is clear from Figure 5.22 that the value of EFS increases with radius of curvature of the system

and approaches saturation for very large values (→∞) of system's radius of curvature considered in the study.

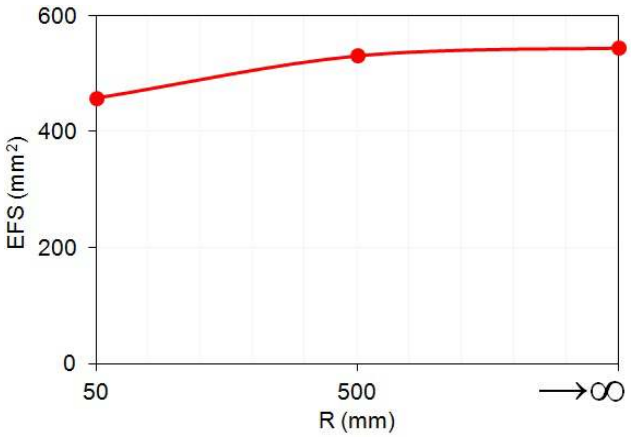

Figure 5.22: Variation of EFS with system's radius of curvature 'R' at z = 10 mm.

5.6 Simulation study of the performance of proposed applicator in close proximity with tri-layered bio-model

The work presented in preceding sections is extended by performing simulation study on the proposed applicator with AMC, which is in close proximity with tri-layered bio-model (skin, fat and muscle layers) as shown in Figure 5.23. The performance of the proposed applicator is now studied through simulation for a tri-layered bio-model consisting of three tri-layered bio-media without and with superficial oval/irregular-shaped abdominal tumor lying inside the muscle tissue. First bio-model pertains to tri-layered bio-media (skin, fat and muscle layers) without tumor. Second bio-model consists of tri-layered bio-media with oval-shaped abdominal /limb tumor lying inside the muscle tissue while the third involves tri-layered bio-media with irregular-shaped abdominal/limb tumor lying inside muscle the muscle tissue. Thicknesses, relative permittivities and densities of biological phantom (muscle)/three layers of bio-media and tumor are given in Table 5.4. The location of oval/irregular-shaped tumor in the muscle medium is provided in Figure 5.25. In all, two tumors of different shapes/sizes were considered in the present study. For heating of tumors designated as tumor1 (oval-shaped) of size 25 mm × 25 mm × 10 mm and tumor2 (irregular-shaped) of size 25 mm × 25 mm × 10 mm, the proposed applicator with AMC designed at 2.45 GHz which is in close proximity with tri-layered bio-media containing these

tumors (one at a time) was considered. A cancerous tumor have higher water content [Michaelson and Lin (1987)] and therefore higher dielectric constant and conductivity. The dielectric property of tri-layered bio-media and tumor is mentioned in Table 5.4.

Table 5.4: Dielectric properties of bio-media [Stuchly and Stuchly (1980)]

Tissue/Tumor	Thickness (mm)	Density (kg/m^3)	ε_r
Skin	1	1130	42-j12
Fat	5	920	5.28-j0.76
Muscle	80	1050	50 - j16
Tumor	10	1050	56-j21.3

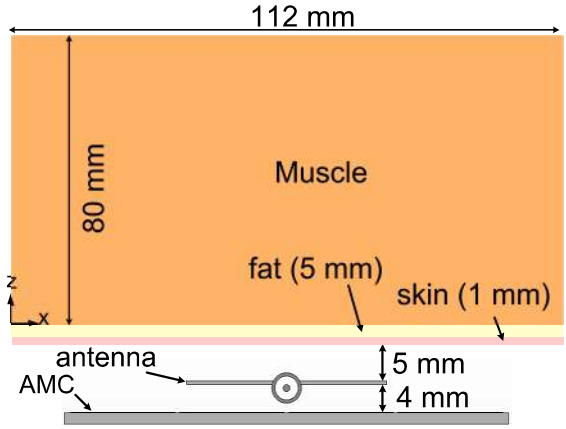

Figure 5.23: Proposed applicator with AMC reflector in close proximity with tri-layered bio-media.

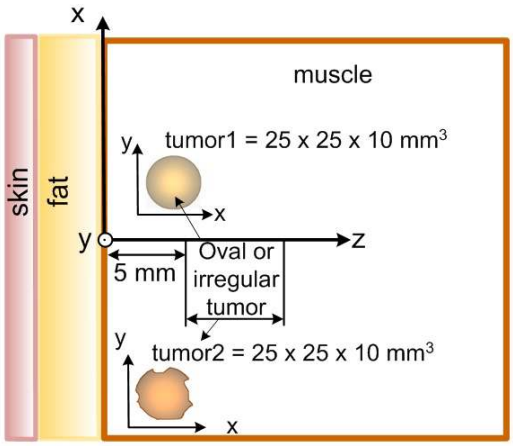

Figure 5.24: Two-dimensional realistic tri-layered bio-model with embedded oval/irregular-shaped tumor.

5.6.1 *SAR distribution without and with tumor*

To observe the effect of tumor embedded in the muscle layer, simulations were performed for the proposed applicator designed at 2.45 GHz which is in

close proximity with tri-layered bio-media without/with embedded tumor and the corresponding SAR distributions are depicted in Figures 5.25. Figure 5.25 shows the simulated variations of normalized SAR distributions in the inhomogeneous tri-layered planar bio-media without/with embedded tumor, along z-direction (for x= y = 0) at 2450 MHz due to the proposed applicator. The values of PD extracted from Figure 5.25 are given in Table 5.5. It can be seen from Table 5.5 that the presence of a tumor does not alter PD significantly. Additionally, it is observed that values of PD in the tri-layered bio-model due to the proposed applicator are sufficient to cover whole tumor depth for effective hyperthermia.

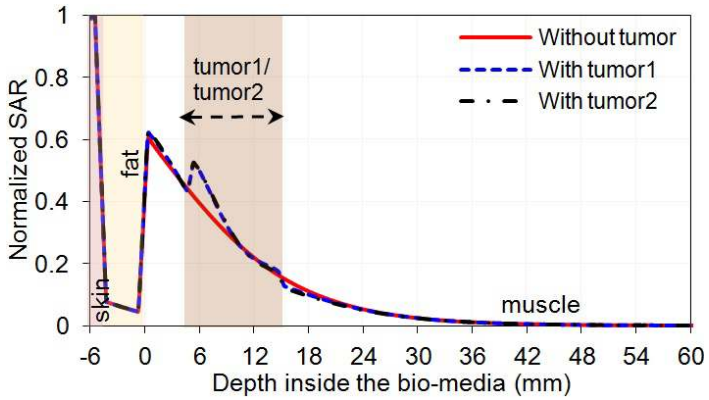

Figure 5.25: Simulated normalized SAR distributions inside the bio-model without and with embedded tumors due to the proposed applicator along z-direction (x = y = 0)**.**

In order to observe the effect of bending on SAR distributions, simulations were performed for three cases involving different values of system's radius of curvature. Case I pertains to both tri-layered bio-model (without/with embedded oval/irregular-shaped tumor) as well as the proposed applicator having radius of curvature 'R' of 50 mm. Case II represents radius of curvature 'R' of 500 mm for the bio-model (without/with embedded oval/irregular-shaped tumor) and the proposed applicator while case III involves planar bio-model (without/with embedded oval/irregular-shaped tumor) and the applicator with 'R' tending to ∞.

The effects of variation in the system's radius of curvature on PD, EFS and SAR patterns were studied through simulation and the results are presented in Figure 5.26-5.29 and Table 5.5. Initially, power fed to the antenna was assumed to be 1 W in the simulation study.

Figure 5.26 shows simulated variations of EFS versus system's radius of curvature due to the proposed applicator with AMC by taking tumor configuration as a parameter. It is observed that in the presence of tumor, EFS increases for a given system's radius of curvature. This may be due to wave scattering/diffraction at the boundary between the tumor and the surrounding muscle tissue since complex permittivity value of tumor is higher as compared to the surrounding muscle tissue. However, the shape of tumor does not alter the value of EFS significantly as system's radius of curvature is decreased. Additionally, the value of EFS first increases at higher rate and then reduces at lower rate as system's radius of curvature is increased from 50 mm to ∞.

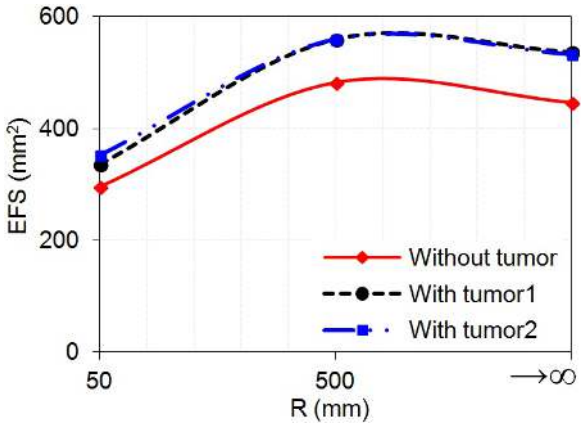

Figure 5.26: Variations of EFS with the system's radius of curvature for inhomogeneous bio-models (without and with embedded tumor) at z = 10 mm.

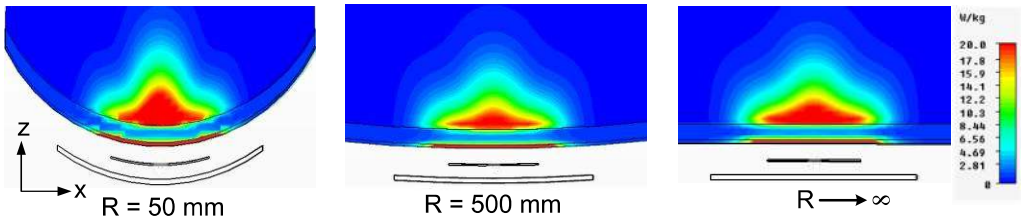

Figure 5.27: SAR patterns in tri-layered bio-model without tumor for various values of system's radius of curvature.

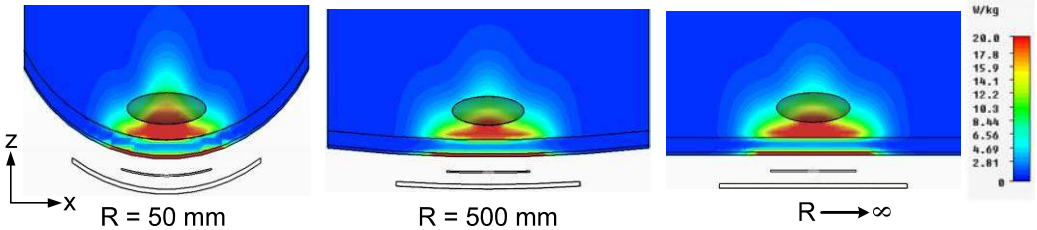

Figure 5.28: SAR patterns in tri-layered bio-model embedded with oval-shaped tumor for various values of system's radius of curvature.

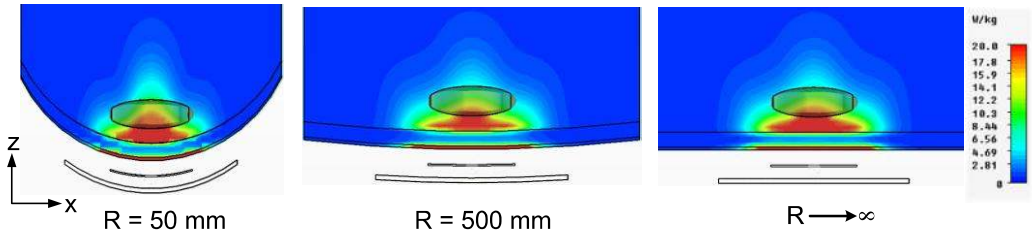

Figure 5.29: SAR patterns in tri-layered bio-model embedded with irregular-shaped tumor for various values of system's radius of curvature.

Figures 5.27, 5.28 and 5.29 show the SAR patterns in the xz-plane respectively for the heterogeneous bio-model without tumor, the heterogeneous bio-model with embedded oval-shaped tumor and the heterogeneous bio-model with embedded irregular-shaped tumor for various values of radius of curvature of the system. It is clear that SAR patterns are symmetrical about z-axis and peak SAR in each case is aligned with the antenna's central axis of radiation. The values of simulated PD, one of the SAR parameters are presented in Table 5.5. Further, it can be observed from Figures 5.27, 5.28 and 5.29 that transverse resolution is improved for lower system's radius of curvature. It can be observed from Table 5.5 that insignificant change in PD in the tri-layered bio-media occurs due to the presence of oval-/irregular-shaped tumor.

5.6.2 *Effects of system curvature on E-field distribution*

To compare the electric field generated in proposed antenna with AMC in close proximity with tri-layered bio-media, near E-field distributions in xz-plane were obtained through simulation for various values of system's radius of curvature (Figure 5.30). It is observed that AMC reflector at the back side of the proposed antenna prevents back radiation and directs the back electric field toward the bio-media for the system's curvatures considered.

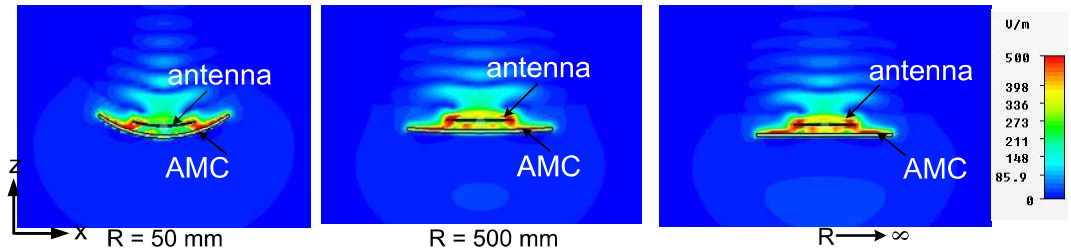

Figure 5.30: E-field distribution in the central regions of proposed antenna with AMC for different values of system's radius of curvature, radiating into tri-layered bio-media.

5.6.3 *Temperature distribution without and with tumor*

The hyperthermia performance of the proposed applicator is characterized through simulation for inhomogeneous tri-layered bio-models fed through proposed applicators. The thermal simulation was performed by CST multi-physics simulator software at an initial temperature of 37^{o} C. The thermal parameters of the bio-media used in simulation are same as given in chapter 2.

It has been observed through thermal simulation study on tri-layered bio-model without tumor that by varying the input power, the desired temperature range (41–45°C) for effective hyperthermia was achieved for input power level of 2.6 W for the proposed antenna-AMC combination designed at 2.45 GHz. The details of this study are not presented here as these have already been provided in preceding chapters for other types of applicators.

Figure 5.31 shows the cross-sectional profiles of temperature distribution in transverse planes in the superficial tumor present in the realistic tri-layered bio-model owing to the proposed applicator for various values of radius of curvature of bio-model and the proposed applicator to which 2.6 W optimum power was fed. It can be seen from Figure 5.31 that desired temperature range (41–45°C) is maintained in the oval-/irregular-shaped tumor for effective hyperthermia.

The values of peak temperature elevation (PTE), heating area, and the depth at which temperature elevation reduces to half of the maximum with respect to initial temperature (=ΔT/2) in the realistic tri-layered bio-models (obtained through thermal simulation) for various values of system's radius of curvature are also given in Table 5.5. It is observed from Table 5.5 that presence of tumor increases PTE in the tissue. It can also be noted from Table 5.5 that the presence or absence of tumor has insignificant effect on heating depth at ΔT/2. Additionally, it is also observed from Table 5.5 that heating area increases due to the presence of tumor. This may have been caused due to, scattering/diffraction of the wave from the boundary of tumor and surrounding normal tissue.

Moreover, heating area first reduces and then increases with increase in system's radius of curvature.

Table 5.5: Hyperthermia performance of the proposed applicator for various values of system's radius of curvature

Curvature (mm)	Inhomogeneous model	PD (mm)	PTE (^{o}C)	Heating depth at ΔT/2 (mm)	Heating area[#] {41-45 $^{\circ}$C} (mm^2)
R = 50	Without tumor	22.81	7.69	22.21	544.44
	With oval-tumor	21.98	7.93	22.82	686.66
	With irregular-tumor	21.56	8.09	22.78	743.20
R = 500	Without tumor	22.2	6.93	21.05	321.31
	With oval-tumor	20.5	7.08	22.00	490.09
	With irregular-tumor	20.62	7.12	22.04	527.21
R → ∞	Without tumor	20.59	7.68	20.57	479.72
	With oval-tumor	19.99	7.90	21.45	630.57
	With irregular-tumor	19.19	7.97	21.57	666.57

[#] Heating area are defined at z = 10 mm inside the muscle layer.

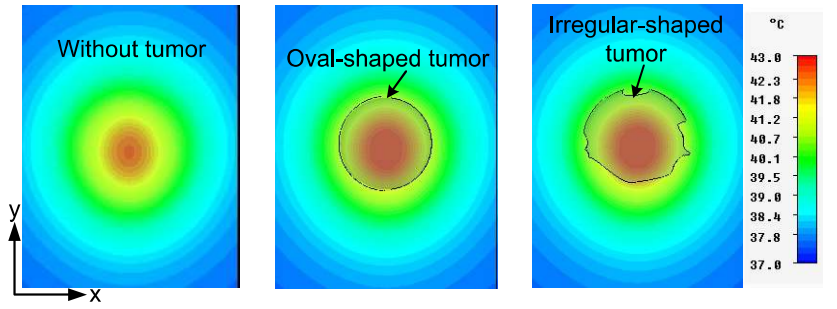

(a)

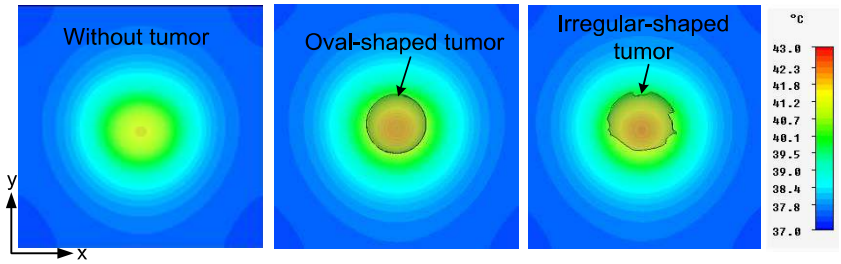

(b)

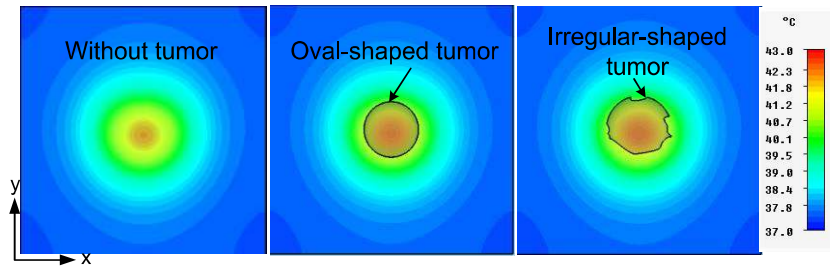

(c)

Figure 5.31: Temperature distributions inside the tri-layered bio-model at 2.45 GHz due to proposed applicator without and with embedded tumor in xy-plane at z = 10 mm for various values of system's radius of curvature (a) R = 50 mm, (b) 500 mm, and (c) R = ∞ (planar).

5.7 Simulation study of the performance of proposed applicator in close proximity with five-layered cylindrical bio-model

The work presented in preceding sections is extended by performing simulation study on the proposed applicator with AMC which is in close proximity with realistic cylindrical bio-model (skin, fat, muscle, cortical bone and bone marrow) as shown in Figure 5.32. Two phantom models of the human limbs are considered in the study: a section of simulated human thigh and a section of simulated human arm. The tissue and tumor dimensions for thigh and arm models without and with embedded tumor are present in Table 5.6 and Figure 5.32. Relative permittivities and densities of five-layered cylindrical bio-media and tumor are given in Table 5.7. It is to be noted that the radii of curvature of antenna-AMC combination considered correspond to respective radii of curvature of the two cylindrical bio-models (thigh- and arm-models).

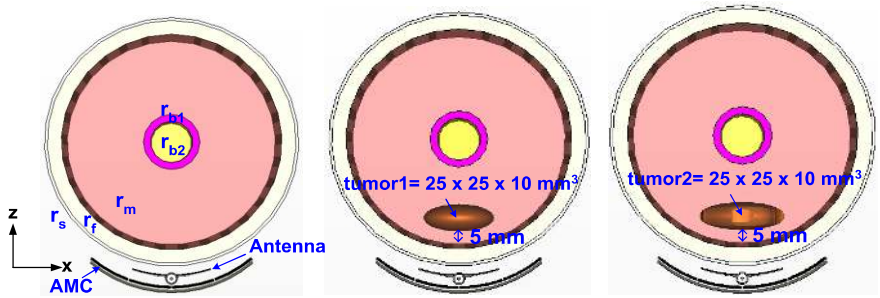

Figure 5.32: Five-layered cylindrical bio-models in close proximity with the proposed applicator.

Table 5.6: Dimensional details of Human limbs model

Tissue dimensions	Thigh model	Arm model
r_s	90	45
r_f	89	44
r_m	84	39
r_{b1}	20	10
r_{b2}	5	2.5

5.7.1 *E-field distribution*

To compare the electric field generated in proposed antenna with AMC in close proximity with two five-layered cylindrical bio-models without tumor (taken one at a time), near E-field distributions in xz-plane were obtained through simulation, for same radius of curvature of antenna-AMC combination as that of

the bio-model considered (Figure 5.33). It is observed from Figure 5.33 that AMC reflector at the back side of the proposed antenna prevents back radiation and directs the back electric field toward the bio-media (thigh and arm) for the given system's radius of curvature considered.

Table 5.7: Dielectric properties of bio-media [Stuchly, and Stuchly (1980), Gabriel (1996)].

Tissue/Tumor	Density (kg/m^3)	ε_r
Skin	1130	42-j12
Fat	920	5.28-j0.76
Muscle	1050	50 - j16
Cortical bone	1990	11.4-2.89
Bone marrow	1040	5.3-j0.69
Tumor	1050	56-j21.3

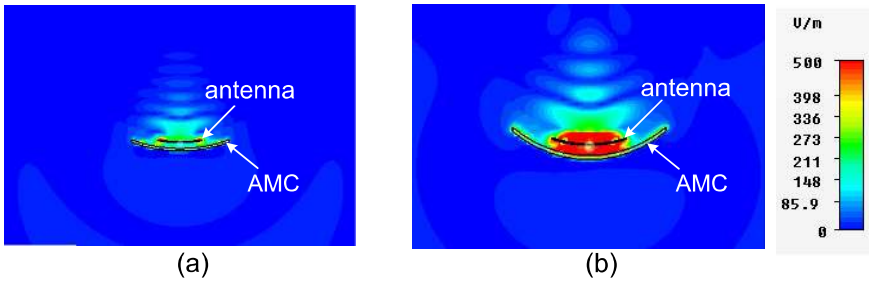

(a) (b)

Figure 5.33: E-field distribution in the central regions of proposed antenna with AMC having same radius of curvature as that of the bio-model, radiating into (a) Thigh model, and (b) Arm model.

5.7.2 *SAR Distribution without and with tumor*

To observe the effect of tumor embedded in the muscle layer, simulations were performed for the proposed applicator designed at 2.45 GHz which is in close proximity with five-layered cylindrical bio-model without/with embedded tumor and the corresponding SAR distributions are depicted in Figures 5.34-5.37. Initially, power fed to the antenna was assumed to be 1 W in the simulation study.

Simulated normalized SAR distributions in the thigh and arm models without/with embedded tumor, along z-direction (for x = y = 0) due to the proposed applicator are presented in Figure 5.34(a) and (b) respectively. Figure 5.35(a) and (b) illustrates the normalized SAR distributions in the aforesaid configurations of bio-model along x-/y-direction due to the proposed applicator. The values of PD and EFS extracted from Figures 5.34 and 5.35 are given in

Table 5.8. It can be seen from Table 5.8 that the presence of a tumor does not alter PD and EFS (in the central region of tumor) significantly in each case.

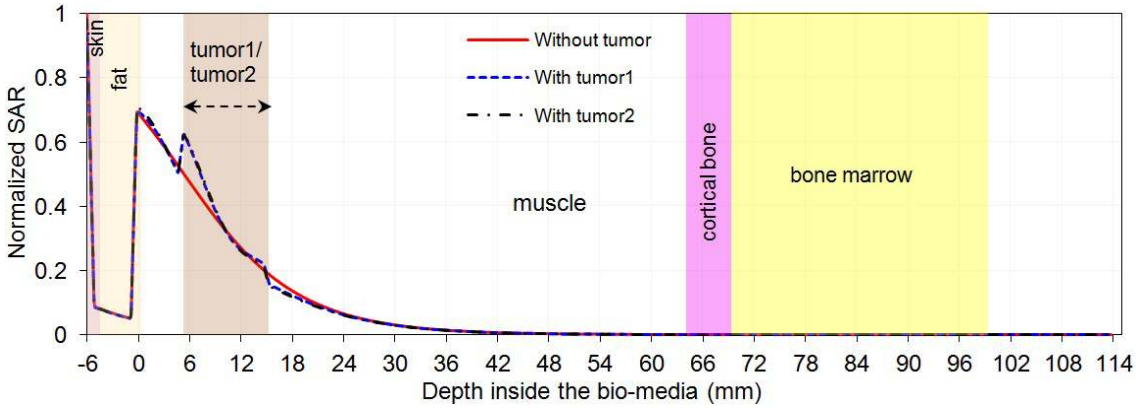

(a)

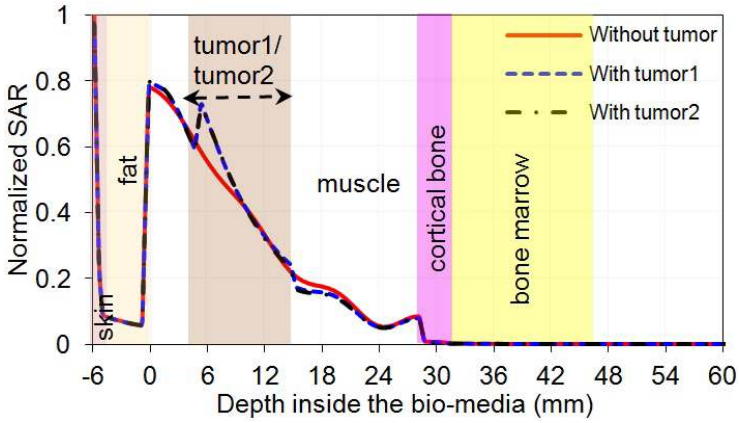

(b)

Figure 5.34: Simulated normalized SAR distributions in the five-layered cylindrical bio-media without and with embedded oval-/irregular-shaped tumor due the proposed applicator along z-direction (x = y = 0) in (a) thigh-model, and (b) arm-model.

Figures 5.36 and 5.37 show the SAR patterns in the xz-plane respectively for the thigh-model without and with embedded tumor and the arm-model without and with embedded tumor respectively. It is clear from Figures 5.36 and 5.37 that SAR distributions are symmetrical about z-axis and peak SAR in each case is aligned with the antenna's central axis of radiation. Table 5.8 summarizes the SAR parameters (PD and EFS) for thigh and arm models without/with embedded tumor. It can be observed from Table 5.8 that insignificant change in PD and EFS in the tri-layered bio-media due to the presence of oval-/irregular-shaped tumor.

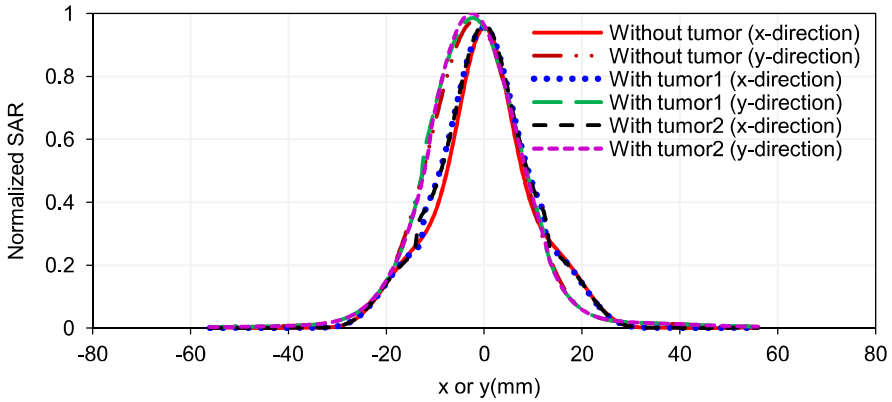

(a)

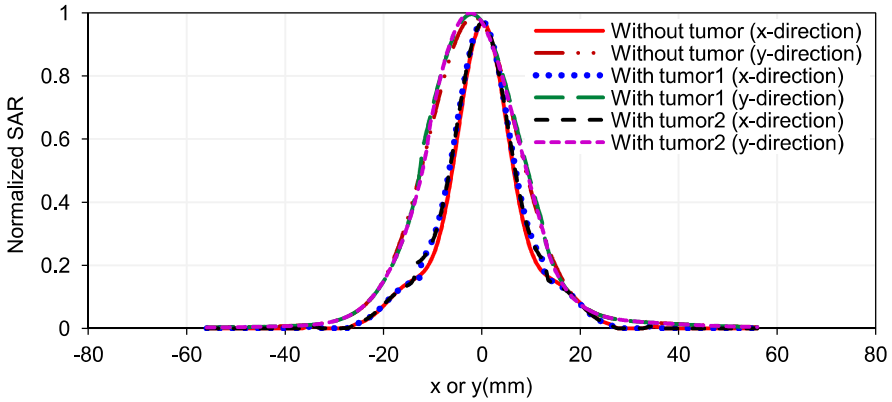

(b)

Figure 5.35: Simulated normalized SAR distributions in the five-layered cylindrical bio-media without and with embedded oval-/irregular-shaped tumor due the proposed applicator along x-/y-direction (z = 10 mm) in (a) thigh-model, and (b) arm-model.

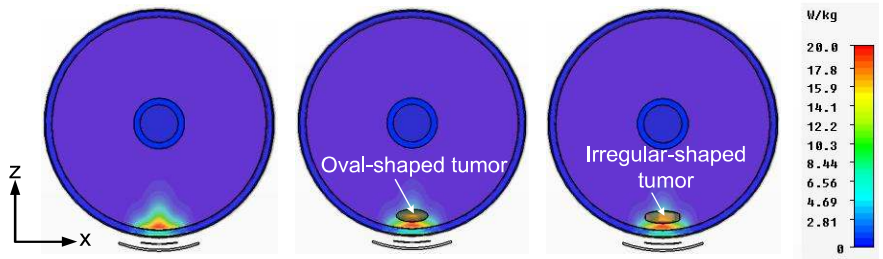

Figure 5.36: SAR patterns in thigh-model without and with embedded oval-/irregular-shaped tumor due to the proposed applicator.

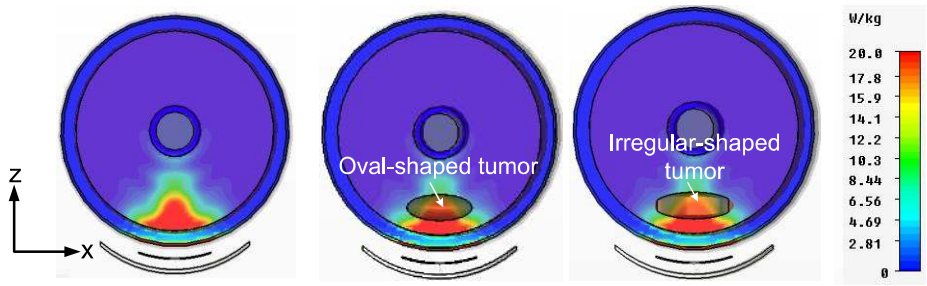

Figure 5.37: SAR patterns in arm-model without and with embedded oval-/irregular-shaped tumor due the proposed applicator.

5.7.3 *Temperature distribution without and with tumor*

In order to characterize the hyperthermia treatment system, the proposed applicator designed at 2.45 GHz was used in simulation to feed microwave power to the cylindrical tissue as shown in Figure 5.32. The thermal simulation was performed by CST multi-physics simulator software at an initial temperature of 37 ^{o}C. The thermal parameters of the tissue used in BHE equation are given in Table 5.9.

It has been observed through thermal simulation study that for effective hyperthermia the desired temperature range (41–45°C) in the thigh and arm models were achieved for 3.5 and 2.2 W input power respectively.

Figure 5.38(a) and (b) show the cross-sectional profiles of temperature distribution in transverse planes in the superficial irregular tumor present in the realistic tri-layered bio-model owing to the proposed applicator for thigh and arm-models respectively. It can be seen from Figure 5.38 that desired temperature range (41–45°C) is maintained in the oval/irregular-shaped tumor for effective hyperthermia.

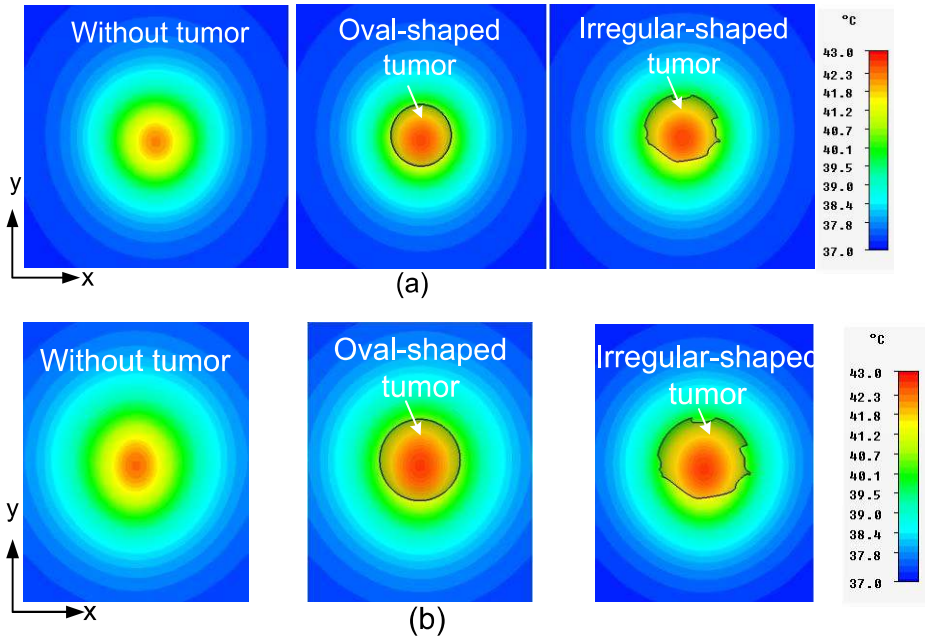

Figure 5.38: Temperature distribution in the five-layered cylindrical bio-media without and with embedded oval-/irregular-shaped tumor (z = 10 mm) due the proposed applicator in (a) thigh-model, and (b) arm-model.

The values of heating area, and the depth at which temperature elevation reduces to half of the maximum with respect to initial temperature (=ΔT/2) in the realistic five-layered bio-models (obtained through thermal simulation) are also given in Table 5.8. It is observed from Table 5.8 that the presence or absence of tumor has insignificant effect on heating depth at ΔT/2. Additionally, it is also observed from Table 5.8 that heating area increases due to presence of tumor. Further, differences in heating characteristics of thigh and arm bio-models are observed. This illustrates the importance of considering two cylindrical bio-models for simulated human limbs.

Table 5.8: Hyperthermia performance of the proposed applicator in thigh and arm models

Model type		PD (mm)	EFS (mm^2)	Heating depth at ΔT/2* (mm)	Heating area* (mm^2)
Thigh	Without tumor	24.1	16.2 × 21.6	20.98	20.45 × 21.18
	With tumor1	23.3	18.9 × 21.82	21.93	23.49 × 23.9
	With tumor2	23	18.2 × 21.5	21.95	24.45 × 24.39
Arm	Without tumor	26.6	12.8 × 21.58	21.27	18.6 × 22.27
	With tumor1	26.16	13.54 × 22.06	21.29	22.21 × 24.68
	With tumor2	26	13.2 × 21.24	22.1	22.55 × 25.43

*For thigh model, optimize input power=3.5 W

*For Arm model, optimize input power=2.2 W

Table 5.9: Thermal parameters of bio-media for the BHE [Gong and Wang (2009), Zhangwei *et al.* (2007)]

Tissue type	ρ (Kg/m^3)	C (KJ/Kg^0C)	K (W/m^0C)	A_0 (W/m^3)	B ($W/m^{3o}C$)
Skin	0.42	3.5	0.42	1620	9100
Fat	920	2.5	0.25	300	1700
Muscle	1050	3.6	0.5	480	2700
Cortical bone	1990	1.3	0.4	610	3400
Bone marrow	1040	2.7	0.22	5700	32000
Tumor	1050	3.6	0.5	480	675

5.8 Conclusion

Microstrip slot antenna with AMC as back plane has been investigated through simulation and experimentally for hyperthermia application at 2.45 GHz. The study involved determination of SAR and temperature distributions in a planar biological phantom/realistic planar tri-layered bio-media/realistic curved tri-layered/five-layered bio-media without and with embedded oval-/irregular-shaped tumor due to the proposed applicator. The proposed microstrip-slot antenna-AMC combination is compact, efficient, focused and provides greater PD for effective heating of small superficial tumors. It is also be inferred that as compared with the antenna-conventional PEC combination, the proposed antenna-AMC combination is of lower profile and provides greater PD as well as wider EFS. Furthermore, the proposed microstrip slot antenna with AMC reflector provides most of the desirable features of the hyperthermia applicator such as enhanced PD, relative insensitivity to variation in the dielectric property of muscle medium, and maintaining conformality. Additionally, it has been observed that EFS decreases when the applicator was bent. This effect is more pronounced for lower radius of curvature of the bio-models/proposed applicator. The temperature distributions in the realistic bio-models obtained through thermal simulation indicate that the proposed applicator designed at 2.45 GHz with 2.6 W input power can be used as effective hyperthermia applicators for oval-and irregular-shaped small tumors in superficial abdominal region of the body. However, for the treatment of tumor in limb portions of the body, it has been found through simulation that desired temperature range (41–45°C) for effective hyperthermia in thigh and arm models have been obtained for 3.5 and 2.2 W optimum input power levels respectively.